Lighting a better future: the virucidal effects of 405 nm visible light on SARS-CoV-2 and influenza A virus.

Raveen Rathnasinghe[1,2,3], Sonia Jangra[1,2], Lisa Miorin[1,2], Michael Schotsasert[1,2], Clifford Yahnke[6#], Adolfo García-Sastre[1,2,4,5#1]

[1]Department of Microbiology, Icahn School of Medicine at Mount Sinai, New York, NY 10029, USA

[2]Global Health and Emerging Pathogens Institute, Icahn School of Medicine at Mount Sinai, New York, NY 10029, USA

[3]Graduate School of Biomedical Sciences, Icahn School of Medicine at Mount Sinai, New York, NY 10029, USA

[4]Department of Medicine, Division of Infectious Diseases, Icahn School of Medicine at Mount Sinai, New York, NY 10029, USA

[5]The Tisch Cancer Institute, Icahn School of Medicine at Mount Sinai, New York, NY 10029, USA
[6] Kenall Manufacturing, Kenosha, WI 53144

[#]Correspondence: cliff.yahnke@kenall.com , adolfo.garcia-sastre@mssm.edu

Abstract

Germicidal potential of specific wavelengths within the electromagnetic spectrum is an area of growing interest. While ultra-violet (UV) based technologies have shown satisfactory virucidal potential, the photo-toxicity in humans coupled with UV associated polymer degradation limit its use in occupied spaces. Alternatively, longer wavelengths with less irradiation energy such as visible light (405 nm) have largely been explored in the context of bactericidal and fungicidal applications. Such studies indicated that 405 nm mediated inactivation is caused by the absorbance of porphyrins within the organism creating reactive oxygen species which result in free radical damage to its DNA and disruption of cellular functions. The virucidal potential of visible-light based technologies has been largely unexplored and speculated to be not effective given the lack of porphyrins in viruses. The current study demonstrated increased susceptibility of

lipid-enveloped respiratory pathogens of importance such as SARS-CoV-2 (causative agent of COVID-19) as well as the influenza A virus to 405nm, visible light in the absence of exogenous photosensitizers, indicating a potential porphyrin-independent alternative mechanism of visible light mediated viral inactivation. Given that visible light is generally safe to humans, our results support further exploration of the use of visible light technology for the application of continuous decontamination in areas within hospitals and/or infectious disease laboratories, specifically for the inactivation of respiratory pathogens such as SARS-CoV-2 and Influenza A.

Key words – Visible light, 405nm, Virucidal, SARS-CoV-2, Influenza, inactivation

Introduction

The severe-acute respiratory syndrome corona virus 2 (SARS-CoV-2), the causative agent of the COVID-19 pandemic, is a member of the beta-coronavirus family and it emerged at the end of 2019 in the Hubei province in Wuhan China[1]. By late February 2021, more than 112 million cases had been reported while accounting for approximately 2.5 million deaths, underscoring the rapid dissemination of the virus on a global scale[2]. As a complement to standard precautions such as handwashing, masking, surface disinfection, and social distancing, other enhancements to enclosed spaces such as improved ventilation and whole-room disinfection are being considered by segments beyond acute healthcare such as retail, dining, and transportation[3].

Initial guidance from health authorities such as the CDC and WHO on environmental transmission focused on contaminated surfaces as fomites[4]. Data pertaining to the survival of SARS-CoV-2 and other related coronaviruses to date has indicated that virions are able to persist on fomites composed of plastic[5], wood[6], paper[5], metal[7] and glass[8] potentially up to nine days. Recent studies have suggested that SARS-CoV-2 may also remain viable approximately at least three days in such surfaces and another two studies showed that at room temperature (20-25°C), a 14-day time-period was required to see a 4.5-5 Log_{10} of the virus[9, 10].

Since the start of the pandemic, transmission of the virus by respiratory droplets and aerosols has become an accepted method of transmission although the relative impact of each mode of transmission is the subject of much debate. Nevertheless, enclosed

spaces with groups of people exercising or singing have been associated with increased transmission. The half-life survival of SARS-CoV-2 in this type of environment has been estimated between 1-2 hours[6, 11, 12].

Taking this information into consideration, several methods have been evaluated to effectively inactivate SARS-CoV-2. Chemical methods, which focus on surface disinfection, utilize 70% alcohol and bleach and their benefits are well established. These methods are also episodic (or non-continuous) meaning that in-between applications, the environment is not being treated[13].

In addition to chemicals, one of the most utilized methods for whole-room disinfection is germicidal ultra-violet C (UVC; ~254 nm)[14]. This technology is well established[15] and has been shown to inactivate a range of pathogens including bacteria[16], fungi[17] and viruses[18]. The mechanism of action of UVC is photodimerization of genetic material such as RNA (relevant for SARS-CoV2 and IAV) and DNA (relevant for DNA viruses and bacterial pathogens, among others)[19]. Unfortunately, this effect has been associated with deleterious effects in exposed humans such as photokeratoconunctivitis in eyes and photodermatitis in skin[20]. For these reasons, UVC irradiation requires safety precautions and cannot be used to decontaminate fomites and high contact areas in the presence of humans[21].

Germicidal properties of violet-blue visible light (380-500 nm), especially within the range of 405 to 450 nm wavelengths have been appreciated as an alternative to UVC irradiation in whole-room disinfection scenarios where it has shown reduction of bacteria[22, 23] in occupied rooms and reductions in surgical site infections[24]. Although 405 nm or closely related wavelengths have been shown to be less germicidal than UVC, its

92 inactivation potential has been assessed in pathogenic bacteria such as *Listeria* spp
93 and *Clostridium* spp[24, 25], and in fungal species such as *Saccharomyces* spp and
94 *Candida* spp[26] . It is thought that the underlying mechanism of blue-light mediated
95 inactivation is associated with absorption of light via photosensitizers such as
96 porphyrins which results in the release of reactive oxygen species (ROS) [27, 28]. The
97 emergence of ROS is associated with direct damage to biomolecules such as proteins,
98 lipids and nucleic acids which are essential constituents of bacteria, fungi and viruses.
99 Further studies have shown that ROS can also lead to the loss of cell membrane
100 permeability mediated by lipid oxidation[29]. Given the lack of endogenous
101 photosensitizers such as porphyrins in virions, efficient decontamination of viruses (both
102 enveloped and non-enveloped) may require the addition of exogenous
103 photosensitizers[23]. With the use of media suspensions containing both endogenous
104 and/or exogenous photosensitizers, inactivation of viruses such as feline calcivirus
105 (FCV)[30], viral hemorrhagic septicemia virus (VHSV)[31] and murine norovirus-1[32] has
106 demonstrated the virucidal potency of 405 nm visible light. Of note, most studies virus
107 inactivation studies have been performed in media containing porphyrins. In the current
108 study, we show the impact of 405 nm irradiation on inactivation of SARS-CoV-2 and
109 influenza A H1N1 viruses without the use of photosensitizers, supporting the possible
110 use of 405 nm irradiation as a tool to confer continuous decontamination of respiratory
111 pathogens such as SARS-CoV-2 and influenza A viruses. We further show the
112 increased susceptibility of lipid-enveloped viruses for irradiation in comparison to non-
113 enveloped viruses, further characterizing the virucidal effects of visible light.

114 **Materials and methods.**

115 **405 nm Exposure System**

116 The visible light disinfection product used in this study was Indigo-Clean from Kenall
117 Manufacturing. The product form factor selected was a 6” downlight (M4DLIC6) to allow
118 for use within a BSL-3 rated containment hood. Within the hood, the distance between
119 the face of the fixture and the sample was 10”- much less than the normal 1.5m used in
120 normal, whole-room disinfection applications. The output of the fixture was modified
121 electronically during its manufacture to match this difference and ensure that the
122 measurements would represent the performance of the device in actual use. For the
123 range of output used in this study, multiple discrete levels were created using pulse
124 width modulation within the LED driver itself. These levels were made to be individually
125 selectable using a simple knob on the attached control module.

126 As expected, the amount of visible light within the 400nm-420nm bandwidth is a
127 measurement of the “dose” delivered to the target organism, measured in $mWcm^{-2}$, is
128 used to quantify this relationship similar to that used in UV disinfection applications.

129 To fully examine this effect, a range of irradiance values were used representing actual
130 product deployment conditions in occupied rooms. The lowest value (0.035 $mWcm^{-2}$)
131 represents a single-mode, lower wattage used in general lighting applications while the
132 highest value (0.6 $mWcm^{-2}$) represents a dual-mode, higher wattage used in critical care
133 applications such as an operating room.

134 The device was placed in a rig to ensure a consistent distance (10”) between the fixture
135 and the samples. The output of the fixture in the test rig was measured using a Stellar-
136 RAD Radiometer from StellarNet configured to make wavelength and irradiance

measurements from 350nm-1100nm with < 1nm spectral bandwidth using a NIST traceable calibration. To ensure that the regular white light portion of the illumination (which is non-disinfecting) was not measured, the measurement was electronically limited to a 1nm bandwidth over the 400nm-420nm range. The normalized spectral profile is shown in Fig. 1 below. The absolute value of the measurement was determined using a NIST traceable calibration as previously described.

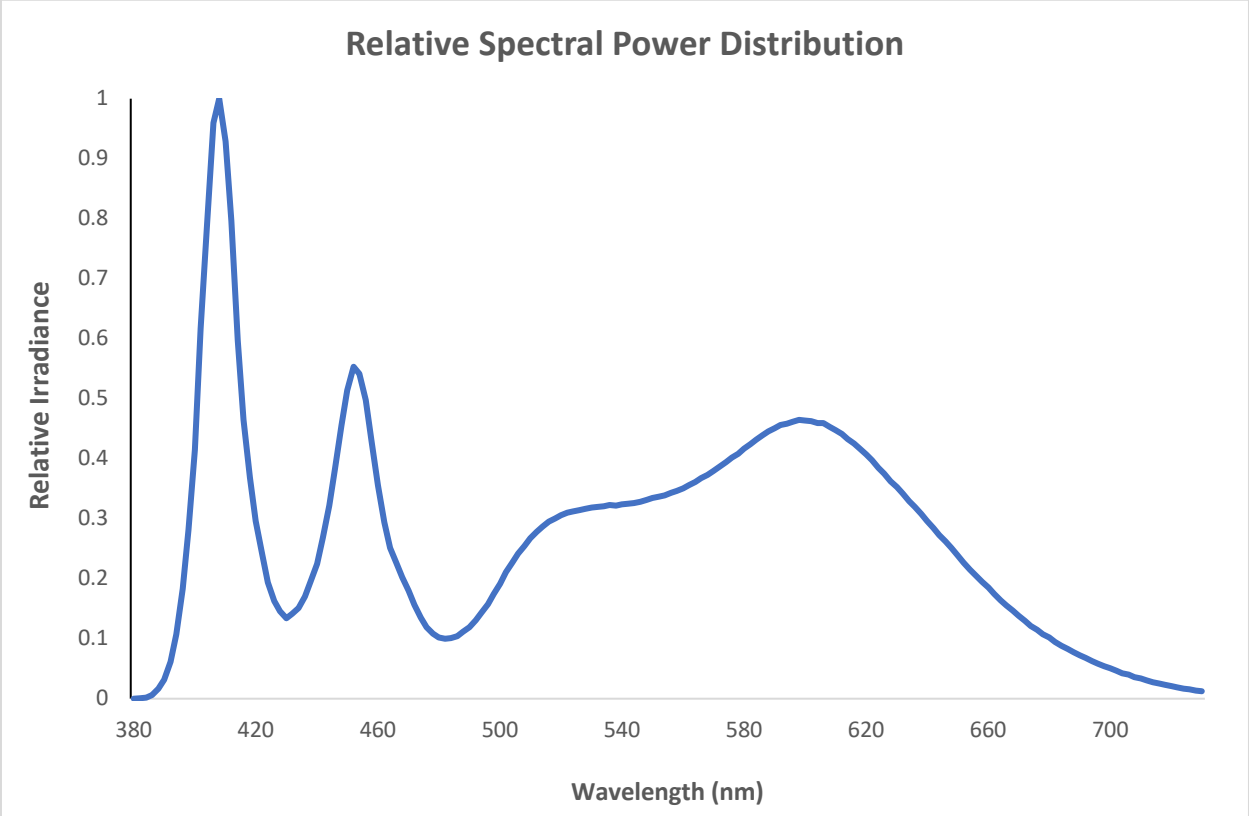

Figure 1. Normalized spectral power distribution for Indigo-Clean M4DLIC6 showing peak irradiance at 405nm.

148 **Cells and viruses**

149 Vero-E6 cells (ATCC® CRL-1586™, clone E6) were maintained in Dulbecco's Modified
150 Eagle Medium (DMEM) complemented with 10% heat-inactivated Fetal Bovine Serum
151 (HI-FBS; PEAK serum), penicillin-streptomycin (Gibco; 15140-122), HEPES buffer
152 (Gibco; 15630-080) and MEM non-essential amino-acids (Gibco; 25025CL) at 37°C with
153 5% CO2. Vero-CCL81 (ATCC® CRL-81™) cells and MDCK cells (ATCC® CCL-34)
154 were cultured in DMEM supplemented with 10% HI-FBS and penicillin/streptomycin at -
155 37ºC with 5% CO2. All experiments involving SARS-CoV2 (USA-WA1/202, BEI
156 resource – NR52281) were conducted within a biosafety-level 3 (BSL3) containment
157 facility at Icahn school of medicine at Mount Sinai by trained workers upon authorization
158 of protocols by a biosafety committee. Amplification of SARS-CoV-2 viral stocks was
159 done in Vero-E6 cell confluent monolayers by using an infection medium composed of
160 DMEM supplemented with 2% HI-FBS, Non-essential amino acids (NEAA), Hepes and
161 penicillin-streptomycin at 37°C with 5% CO2 for 72 hours. Influenza A virus used here
162 was generated using plasmid based reverse genetics system as previously described[33].
163 The backbone used in the study was A/Puerto Rico/8/34/Mount Sinai(H1N1) under the
164 GenBank accession number AF389122. IAV-PR8 virus was grown and titrated in MDCK
165 as previously described[33]. As a non-enveloped virus, the cell culture adapted murine
166 Encephalomyocarditis virus (EMCV; ATCC® VR-12B) was propagated and titrated in
167 Vero-CCL81 cells with DMEM and 2% HI-FBS and penicillin-streptomycin at 37°C with
168 5% CO2 for 48 hours[34].

169 **405nm inactivation of viruses**

170 The SARS-CoV-2 virus was exclusively handled at the Icahn school of Medicine BSL-3
171 and studies involving IAV and EMCV were handled in BSL-2 conditions. Indicated PFU
172 amounts were mixed with sterile 1X PBS and were irradiated in 96 well format cell
173 culture plates in triplicates. In these studies, A starting dose of $5x10^5$ PFU for SARS-
174 CoV-2 and starting doses of $1x10^5$ PFU for IAV and EMCV were used. The final
175 volumes for inactivation were 250 µl per replicate. The untreated samples were
176 prepared the same way and were left inside the biosafety cabinet isolated from the
177 inactivation device at room temperature. The plates were sealed with qPCR plate
178 transparent seal and an approximate 10% reduction of the intensity was observed due
179 to the sealing film. The distance from the lamp and the samples was measured to be
180 10". All samples were extracted at indicated times and were frozen at -80°C and were
181 thawed together for titration via plaque assays.

182 **Plaque assays**

183 Confluent monolayers of Vero-E6 cells in 12-well plate format were infected with 10-fold
184 serially diluted samples in 1X phosphate-buffered saline (PBS) supplemented with
185 bovine serum albumin (BSA) and penicillin-streptomycin for an hour while gently
186 shaking the plates every 15 minutes. Afterwards, the inoculum was removed, and the
187 cells were incubated with an overlay composed of MEM with 2% FBS and 0.05% Oxoid
188 agar for 72 hours at 37°C with 5% CO_2. The plates were subsequently fixed using 10%
189 formaldehyde overnight and the formaldehyde was removed along with the overlay.
190 Fixed monolayers were blocked with 5% milk in Tris-buffered saline with 0.1% tween-20
191 (TBS-T) for an hour. Afterwards, plates were immunostained using a monoclonal
192 antibody against SARS-CoV2 nucleoprotein (Creative-Biolabs; NP1C7C7) at a dilution

193 of 1:1000 followed by 1:5000 anti-mouse IgG monoclonal antibody and was developed
194 using KPL TrueBlue peroxidase substrate for 10 minutes (Seracare; 5510-0030). After
195 washing the plates with distilled water, the number of a plaques were counted. Plaque
196 assays for IAV and EMCV were done in a similar fashion. For IAV, confluent
197 monolayers of MDCK cells supplemented with MEM-based overlay with TPCK-treated
198 trypsin was used. For EMCV, Vero-CCL81 cells were used to do plaque assays in 6
199 well plate format. Plaques for IAV and EMCV were visualized using crystal violet. Data
200 shown here is derived from three independent experimental setups.

201 **Results.**

202 **Dose and time dependent inactivation of SARS-CoV-2 in the absence of**
203 **photosensitizers.**

204 The lowest irradiation dose of 0.035 $mWcm^{-2}$ was applied for SARS-CoV-2 and when
205 compared to the initial input (T_0) of ~$5x10^5$ PFU, a reduction of 55.08% was seen as
206 early as 4 hours and after 24 hours of irradiation, an inactivation of 90.17%
207 (approximately 10 times reduction in infectivity) was observed for SARS-CoV-2 via
208 plaque assays (Figure 2A). A slightly higher dose of 0.076$mWcm^{-2}$ resulted in a
209 reduction of 98.22% (56 times) after 24 hours when compared to the original input at T_0
210 (Figure 2B). Subsequent increase of the irradiation dose to 0.150 $mWcm^{-2}$ resulted in a
211 reduction of 63.64% after 4 hours which then reached 96.21% after 12 hours. Irradiation
212 for 24 hours at 0.150 $mWcm^{-2}$ suggested a total reduction of 99.61% (256 times) for
213 SARS-CoV-2 (Figure 2C). As a final experiment, a high irradiation dose of 0.6 $mWcm^{-2}$
214 was used to assess the inactivation potential within a much shorter time frame.
215 Irradiation for one hour resulted in a reduction of 71.52% which reached 91.15% after

four hours and 99.74% (385 times) after 8 hours in comparison to the initial input (T_0) (Figure 2 D and E). All experimental conditions demonstrated the stability of untreated SARS-CoV-2 which was left at room temperature in PBS, as shown by the marginal reduction of viral titer over time.

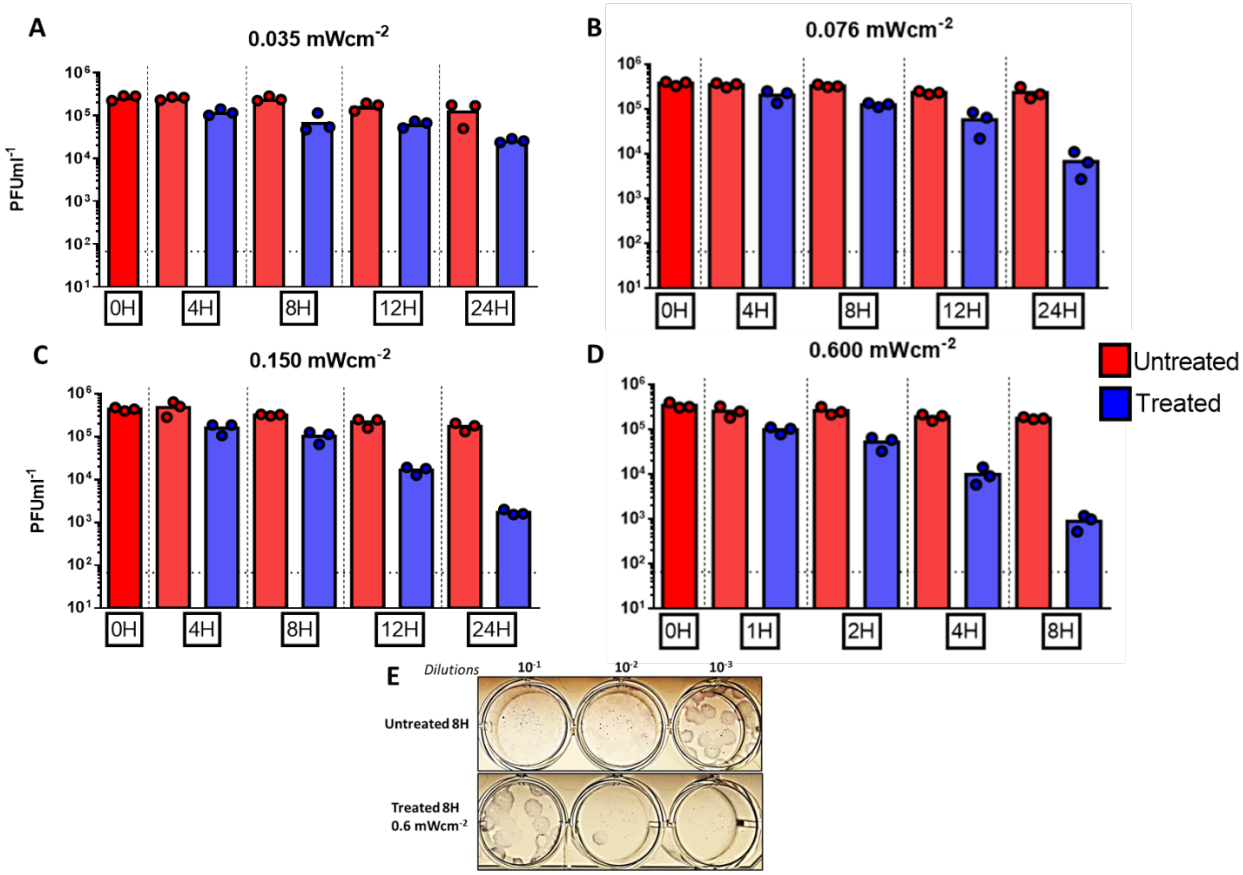

Figure 2. Dose and time dependent inactivation of SARS-CoV-2 virus in PBS by 405 nm irradiation. A. A dose of 0.035 $mWcm^{-2}$ or **B.** a dose of 0.076 $mWcm^{-2}$ or **C.** a dose of 0.150 $mWcm^{-2}$ or **D.** a dose of 0.6 $mWcm^{-2}$ was applied to irradiate samples at 405 nm over a course of 24 while sampling at 4, 8, 12 and 24 hours (for A, B and C) or over a course of 8 hours while sampling at 1, 2, 4 and 8 hours (D) was done in independent triplicates. Blue bars indicate treated samples and red bars correspond to the untreated equivalent that was left at the biosafety cabinet under the same conditions while not subjecting to irradiation. Data shown as $PFUml^{-1}$ in triplicate assessed by plaque assay. **E.** Plaque phenotype comparison from one independent experiment at an irradiation dose of 0.6 $mWcm^{-2}$. Fixed and blocked plaques were immunostained using anti-NP antibody before developing using TrueBlue reagent.

229 **Influenza A virus is susceptible to 405 nm inactivation in the absence of**
230 **photosensitizers.**

231 Given the observations derived from SARS-CoV-2, a separate inactivation study using a
232 different lipid-enveloped RNA virus was conducted by using influenza A Puerto Rico
233 (A/H1N1/PR8-Mount Sinai) virus strain. Irradiation with a high dose of 0.6 $mWcm^{-2}$
234 suggested a time dependent reduction of infectivity of 31.11%, 63.33%, 81.56% and
235 98.49% (66 tiems) at 1, 2, 4 and 8 hours respectively (Figure 3A and 3B).

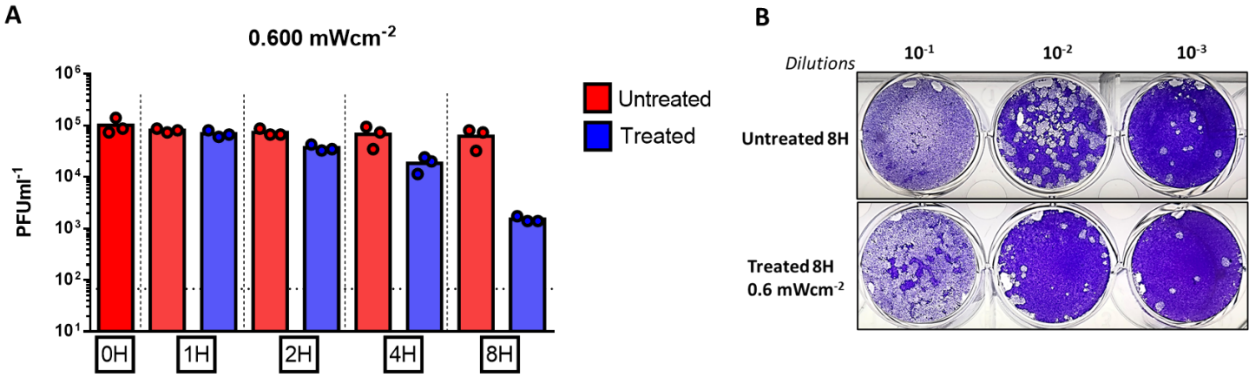

236

237 **Figure 3 Inactivation of Influenza A virus in PBS by 405 nm irradiation. A.** A dose of 0.6 $mWcm^{-2}$ was applied to irradiate
238 samples at 405 nm over a course 8 hours while sampling at 1, 2, 4 and 8 hours (done in independent triplicates). Blue bars indicate
239 treated samples and red bars correspond to the untreated equivalent that was left at the biosafety cabinet under the same
240 conditions while not subjecting to irradiation. Data shown as $PFUml^{-1}$ in triplicate assessed by plaque assay. **B.** Plaque phenotype
241 comparison from one independent experiment at an irradiation dose of 0.6 $mWcm^{-2}$. Fixed and blocked plaques were stained using
242 crystal violet.

243 The stability of IAV virus at room temperature for a period of 8 hours was found to be
244 the negligible in untreated IAV spiked PBS samples (Figure 3A).

245 **Encephalomyocarditis virus (EMCV) as a model non-enveloped virus indicates**
246 **reduced susceptibility to 405 nm inactivation in the absence of photosensitizers.**

247 In order to better understand the effect of the lipid-envelope in viral inactivation by 405
248 nm irradiation, we used a non-lipid enveloped RNA virus derived from the
249 *Picornaviridae* family. EMCV virus was irradiated at a high dose of 0.6 mWcm^{-2} similar
250 to SARS-CoV-2 and IAV.

251

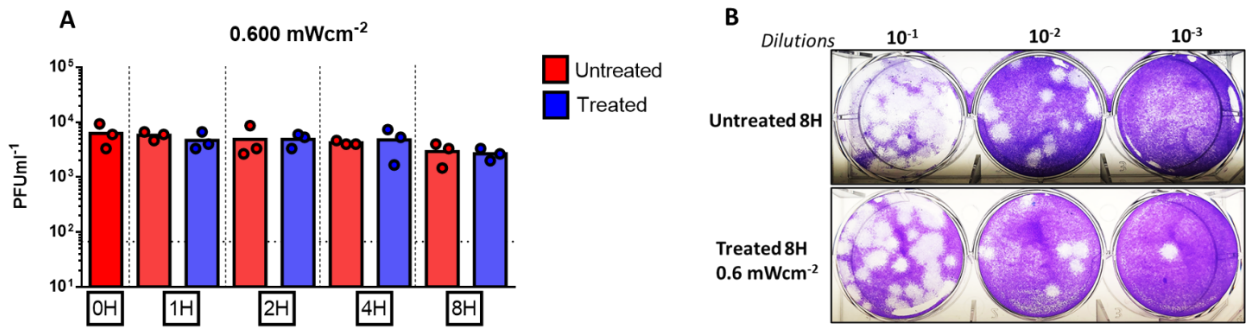

252 **Figure 4. Encephalomyocarditis virus (EMCV) in PBS shows reduced susceptibility to 405 nm irradiation. A.** A dose of 0.6
253 mWcm^{-2} was applied to irradiate samples at 405 nm over a course 8 hours while sampling at 1, 2, 4 and 8 hours (done in
254 independent triplicates). Blue bars indicate treated samples and red bars correspond to the untreated equivalent that was left at the
255 biosafety cabinet under the same conditions while not subjecting to irradiation. Data shown as PFUml^{-1} in triplicate assessed by
256 plaque assay. **B.** Plaque phenotype comparison from one independent experiment at an irradiation dose of 0.6 mWcm^{-2}. Fixed and
257 blocked plaques were stained using crystal violet.

258

259 In this case however, a total reduction of 9.1% (approximately 2 times) in comparison to
260 the initial input (T_0) after 8 hours of irradiation was observed (Fig 4A and 4 B) indicating
261 a lower rate of inactivation in contrast to the lipid-enveloped RNA viruses tested in this
262 study. The plaque reduction at 8 hours did not indicate the same dramatic reduction as
263 observed with the latter studies.

264 Discussion

265 The ongoing SARS-CoV-2 pandemic has affected the day-to-day functions in the entire
266 world, raising concerns not only with regards to therapeutics but also in the context of

267 virus survivorship and decontamination[35]. Taking into consideration the rapid spread of
268 SARS-CoV-2 from person to person by droplets, aerosols, and fomites, whole-room
269 disinfection systems can be viewed as a supplement to best practices for interrupting
270 transmission of the virus.

271 Given the ongoing COVID-19 pandemic, we wanted to explore the impact of 405 nm
272 enriched visible light technology on inactivation of respiratory pathogens such as SARS-
273 CoV-2 and influenza A virus.

274 Without the use of exogenous photosensitizers, we were able to show that irradiation
275 with low intensity (0.035 $mWcm^{-2}$) visible light yielded a total of 55.08% inactivation after
276 four hours and a total of 90.17% inactivation of SARS-CoV-2 after 24 hours. A slightly
277 higher dose (0.076 $mWcm^{-2}$) resulted in 98.22% inactivation after 24 hours while an
278 irradiation dose of 0.150 $mWcm^{-2}$ showed a reduction of 63.64% and 99.61% after four
279 hours and 24 hours of irradiation, respectively. Finally, increasing the dose to 0.6
280 $mwcm^{-2}$ yielded 99.74% after eight hours, indicating a both time and dose dependent
281 inactivation of infectious viruses. We selected conventional plaque assays as the read
282 out to specifically estimate infectious virus titers upon disinfection. Methods based in the
283 quantification of viral RNA via PCR based techniques might be misleading as they
284 detect viral RNA from both infectious and noninfectious virions.

285 SARS-CoV-2 is a lipid-enveloped virus composed of a ssRNA genome and our data
286 indicates its susceptibility to visible light mediated inactivation. To further confirm these
287 observations, we used influenza A virus. which is another human respiratory virus with a
288 lipid envelop and an RNA genome. Upon irradiating for 1 hour at 0.6 $mWcm^{-2}$, we
289 observed a total reduction of 31.11% for the influenza A virus compared to the reduction

290 of 71.52% for SARS-CoV-2 under the same conditions. While both viruses have lipid
291 envelopes, there is clearly a difference here that will require further study. One possible
292 explanation is the difference in the virion size creating a physically smaller cross-section
293 for absorption. (IAV ~120 nm and SARS-CoV-2 ~200 nm)[36, 37]. Nevertheless, both
294 viruses were largely inactivated after eight hours- 98.49% for IAV and 99.74% for
295 SARS-CoV-2. Intriguingly, it was observed that both RNA viruses were able to remain
296 stable at room temperature for at least 24 hours, indicating minimal decay which is
297 consistent with previous studies[35, 38]. We next irradiated a non-enveloped RNA virus,
298 EMCV. Previous results for visible light against non-enveloped viruses demonstrated
299 the need for external photosensitizers such as artificial saliva, blood, feces, etc[30, 35].
300 Without a porphyrin containing medium, we expected little to no inactivation when this
301 virus was irradiated with visible light. For these measurements, we used the highest
302 available irradiance of 0.6 $mWcm^{-2}$. As anticipated, we observed only a 9.1%
303 inactivation after eight hours, however, this appears to be with the statistical precision of
304 the measurement based on the results obtained from shorter irradiations (1, 2, and 4
305 hours). For comparison, a study involving the M13-bacteriophage virus (a non-
306 enveloped virus) showed a 3-Log reduction using an irradiance of $50mWcm^{-2}$ (almost
307 100 times greater than the highest irradiance used in this study) for 10 hours at 425 nm
308 further supporting the idea that non-enveloped viruses may require higher doses of
309 visible light[39].

310 Our study was conducted using a neutral liquid media composed of PBS without any
311 photosensitizers and we were able to show that visible light can indeed inactivate lipid-
312 enveloped viruses, differing from the theory that states that photosensitizers are a

313 requirement for inactivation. Other studies which used visible light-based irradiation
314 have shown similar results in the absence of photosensitizers, indicating the possibility
315 of an alternative inactivation mechanism[23, 25, 30]. Studies have proposed two theories for
316 this observation primarily due to non-405nm wavelengths emitted by the source: 1)
317 some amount of 420-430 nm emitted from the source is contributing to the viral
318 inactivation [40], and 2) the presence of UV-A (390 nm) within the source. This
319 wavelength is known to create oxidative stress upon viral capsids[41].

320 Longer wavelengths, such as 420-430nm, have shown inactivation of the murine
321 leukemia virus (MRV-A) [40]. While this is an intriguing study, it used a broad-spectrum
322 lamp with optical filters to selectively identify the spectrum primarily responsible with
323 their results. Unfortunately, they did not quantify the amount of light (using radiometric
324 units) within the spectrum of interest used to irradiate the virus. While transmission
325 profile of the filters used were provided, it does not take into account the spectral
326 composition of the source itself making any direct quantitative comparison between our
327 studies impossible. It is interesting to note that they did observe viral inactivation in
328 their controls from wavelengths less than 420nm confirming the qualitative findings of
329 our study without confirming the specific use of 405nm. This suggests that the viral
330 inactivation is a likely a broad response (> 20nm) with relative contributions unique to
331 the chemistry of each organism. They also considered much longer exposures (~7
332 days) and much higher illuminance (> 200 lux) than that used in our study although this
333 is again difficult to compare given the lack of radiometric quantification of their light
334 source. It is important to note that the control samples used in our study were exposed
335 to the same overhead (non-405nm) lights as the irradiated samples and our results are

336 the observed difference between the two demonstrating the contribution from 405nm
337 over and above that potentially from 420-430nm. Future experiments can further
338 quantify the potential effect.

339 The other theory, potential UV-A irradiation, was historically applied to lamp-based
340 sources with broad spectral (> 100nm) outputs. Again, the use of LED technology
341 addresses this question as the peak irradiance at 390nm of the device used in this
342 study was < 1% of its peak irradiance at 405nm without the need for any additional
343 filtration. Future experiments can further quantify the potential effect.

344 The results obtained suggest that the performance of visible light against SARS-CoV-2
345 is similar to organisms commonly found in the environment such as *S. aureus*.
346 Previous studies have shown that the visible light irradiance levels used in this study
347 (0.035 $mWcm^{-2}$ to 0.6 $mWcm^{-2}$) reduce bacteria levels in occupied rooms and improve
348 outcomes for surgical procedures. It is therefore reasonable to conclude that visible light
349 might be an effective disinfectant against SARS-CoV-2. More importantly, this
350 disinfection can operate continuously as it is safe for humans based upon the exposure
351 guidelines in IEC 62471[42]. This means that once it has been in use for a period of time,
352 the environment will be cleaner and safer the next time it is occupied by humans.

353 One limitation of this study is that the inactivation assays were performed in static liquid
354 media as opposed to aerosolized droplets. While the use of visible light in air
355 disinfection has been briefly studied where it was shown that its effectiveness increased
356 approximately 4-fold[43], further studies involving dynamic aerosolization are needed to
357 better understand the true potential of visible light mediated viral inactivation.

358 In any case, our study shows the increased susceptibility of enveloped respiratory viral
359 pathogens to 405 nm mediated inactivation in the absence of photosensitizers. The
360 irradiances used in this study are very low and might be easily applied to safely and
361 continuously disinfect occupied areas within hospitals, schools, restaurants, offices and
362 other locations.

363 **Acknowledgments**

364 We thank Randy Albrecht for support with the BSL3 facility and procedures at the ISMMS, and
365 Richard Cadagan for technical assistance. This research was partly funded by CRIP (Center for
366 Research for Influenza Pathogenesis), a NIAID supported Center of Excellence for Influenza
367 Research and Surveillance (CEIRS, contract # HHSN272201400008C); by the generous
368 support of the JPB Foundation, the Open Philanthropy Project (research grant 2020-215611
369 (5384)) and anonymous donors to AG-S, and by a research contract from Kenall Manufacturing
370 to the AG-S lab.

371 **Conflicts of interest**

372 The García-Sastre Laboratory has received research support from Pfizer, Senhwa
373 Biosciences, 7Hills Pharma, Avimex, Blade Therapeutics, Dynavax, ImmunityBio,
374 Nanocomposix and Kenall Manufacturing. Adolfo García-Sastre has consulting
375 agreements for the following companies involving cash and/or stock: Vivaldi
376 Biosciences, Pagoda, Contrafect, 7Hills Pharma, Avimex, Vaxalto, Accurius, Pfizer and
377 Esperovax. RR, CY and AGS have filed for a provisional patent based upon these
378 results.

379 **References**

380 1. Andersen, K. G., Rambaut, A., Lipkin, W. I., Holmes, E. C. & Garry, R. F. The
381 proximal origin of SARS-CoV-2. *Nat. Med.* **26**, 450-452 (2020).

382 2. Worldometer, D. COVID-19 coronavirus pandemic. *World Health Organization,*
383 *www.worldometers.info* (2020).

384 3. Buitrago-Garcia, D. *et al*. Occurrence and transmission potential of asymptomatic and
385 presymptomatic SARS-CoV-2 infections: A living systematic review and meta-analysis.
386 *PLoS medicine* **17**, e1003346 (2020).

387 4. https://www.who.int/news-room/commentaries/detail/modes-of-transmission-of-virus-
388 causing-covid-19-implications-for-ipc-precaution-recommendations.

389 5. Dehbandi, R. & Zazouli, M. A. Stability of SARS-CoV-2 in different environmental
390 conditions. *The Lancet Microbe* **1**, e145 (2020).

391 6. Van Doremalen, N. *et al*. Aerosol and surface stability of SARS-CoV-2 as compared
392 with SARS-CoV-1. *N. Engl. J. Med.* **382**, 1564-1567 (2020).

393 7. Behzadinasab, S., Chin, A., Hosseini, M., Poon, L. & Ducker, W. A. A surface coating
394 that rapidly inactivates SARS-CoV-2. *ACS applied materials & interfaces* **12**, 34723-
395 34727 (2020).

396 8. Chan, K. *et al*. Factors affecting stability and infectivity of SARS-CoV-2. *J. Hosp.*
397 *Infect.* **106**, 226-231 (2020).

398 9. Biryukov, J. *et al*. Increasing Temperature and Relative Humidity Accelerates
399 Inactivation of SARS-CoV-2 on Surfaces. *mSphere* **5**, 10.1128/mSphere.00441-20
400 (2020).

401 10. Aboubakr, H. A., Sharafeldin, T. A. & Goyal, S. M. Stability of SARS-CoV-2 and
402 other coronaviruses in the environment and on common touch surfaces and the
403 influence of climatic conditions: A review. *Transboundary and emerging diseases*
404 (2020).

405 11. Smither, S. J., Eastaugh, L. S., Findlay, J. S. & Lever, M. S. Experimental aerosol
406 survival of SARS-CoV-2 in artificial saliva and tissue culture media at medium and high
407 humidity. *Emerging microbes & infections* **9**, 1415-1417 (2020).

408 12. Schuit, M. *et al*. Airborne SARS-CoV-2 is rapidly inactivated by simulated sunlight.
409 *J. Infect. Dis.* **222**, 564-571 (2020).

410 13. Kampf, G., Todt, D., Pfaender, S. & Steinmann, E. Persistence of coronaviruses on
411 inanimate surfaces and their inactivation with biocidal agents. *J. Hosp. Infect.* **104**, 246-
412 251 (2020).

413 14. Rutala, W. A. & Weber, D. J. Disinfection and sterilization in health care facilities:
414 what clinicians need to know. *Clinical infectious diseases* **39**, 702-709 (2004).

415 15. Rathnasinghe, R. *et al*. Scalable, effective, and rapid decontamination of SARS-
416 CoV-2 contaminated N95 respirators using germicidal ultra-violet C (UVC) irradiation
417 device. *medRxiv* (2020).

418 16. Escombe, A. R. *et al*. Upper-room ultraviolet light and negative air ionization to
419 prevent tuberculosis transmission. *PLoS Med* **6**, e1000043 (2009).

420 17. Nakpan, W., Yermakov, M., Indugula, R., Reponen, T. & Grinshpun, S. A.
421 Inactivation of bacterial and fungal spores by UV irradiation and gaseous iodine
422 treatment applied to air handling filters. *Sci. Total Environ.* **671**, 59-65 (2019).

423 18. Tseng, C. & Li, C. Inactivation of viruses on surfaces by ultraviolet germicidal
424 irradiation. *Journal of occupational and environmental hygiene* **4**, 400-405 (2007).

425 19. Kowalski, W. in *Ultraviolet germicidal irradiation handbook: UVGI for air and surface*
426 *disinfection* (Springer science & business media, 2010).

427 20. Zaffina, S. *et al*. Accidental exposure to UV radiation produced by germicidal lamp:
428 case report and risk assessment. *Photochem. Photobiol.* **88**, 1001-1004 (2012).

429 21. Leung, K. C. P. & Ko, T. C. S. Improper Use of the Germicidal Range Ultraviolet
430 Lamp for Household Disinfection Leading to Phototoxicity in COVID-19 Suspects.
431 *Cornea* **40**, 121-122 (2021).

432 22. Maclean, M. *et al*. Environmental decontamination of a hospital isolation room using
433 high-intensity narrow-spectrum light. *J. Hosp. Infect.* **76**, 247-251 (2010).

434 23. Maclean, M., McKenzie, K., Anderson, J. G., Gettinby, G. & MacGregor, S. J. 405
435 nm light technology for the inactivation of pathogens and its potential role for
436 environmental disinfection and infection control. *J. Hosp. Infect.* **88**, 1-11 (2014).

437 24. Murrell, L. J., Hamilton, E. K., Johnson, H. B. & Spencer, M. Influence of a visible-
438 light continuous environmental disinfection system on microbial contamination and
439 surgical site infections in an orthopedic operating room. *Am. J. Infect. Control* **47**, 804-
440 810 (2019).

441 25. Maclean, M., Murdoch, L. E., MacGregor, S. J. & Anderson, J. G. Sporicidal effects
442 of high-intensity 405 nm visible light on endospore-forming bacteria. *Photochem.*
443 *Photobiol.* **89**, 120-126 (2013).

444 26. Murdoch, L., McKenzie, K., Maclean, M., Macgregor, S. & Anderson, J. Lethal
445 effects of high-intensity violet 405-nm light on Saccharomyces cerevisiae, Candida

446 albicans, and on dormant and germinating spores of Aspergillus niger. *Fungal Biology*
447 **117**, 519-527 (2013).

448 27. Dai, T. *et al*. Blue light for infectious diseases: Propionibacterium acnes,
449 Helicobacter pylori, and beyond? *Drug Resistance Updates* **15**, 223-236 (2012).

450 28. Bumah, V. V. *et al*. Spectrally resolved infrared microscopy and chemometric tools
451 to reveal the interaction between blue light (470 nm) and methicillin-resistant
452 Staphylococcus aureus. *Journal of Photochemistry and Photobiology B: Biology* **167**,
453 150-157 (2017).

454 29. Hadi, J., Dunowska, M., Wu, S. & Brightwell, G. Control Measures for SARS-CoV-2:
455 A Review on Light-Based Inactivation of Single-Stranded RNA Viruses. *Pathogens* **9**,
456 737 (2020).

457 30. Tomb, R. M. *et al*. New proof-of-concept in viral inactivation: virucidal efficacy of 405
458 nm light against feline calicivirus as a model for norovirus decontamination. *Food and*
459 *environmental virology* **9**, 159-167 (2017).

460 31. Ho, D. T. *et al*. Effect of blue light emitting diode on viral hemorrhagic septicemia in
461 olive flounder (Paralichthys olivaceus). *Aquaculture* **521**, 735019 (2020).

462 32. Wu, J. *et al*. Virucidal efficacy of treatment with photodynamically activated
463 curcumin on murine norovirus bio-accumulated in oysters. *Photodiagnosis and*
464 *photodynamic therapy* **12**, 385-392 (2015).

465 33. Martinez-Sobrido, L. & Garcia-Sastre, A. Generation of recombinant influenza virus
466 from plasmid DNA. *J. Vis. Exp.* **(42). pii: 2057. doi**, 10.3791/2057 (2010).

467 34. Carocci, M. & Bakkali-Kassimi, L. The encephalomyocarditis virus. *Virulence* **3**, 351-
468 367 (2012).

469 35. Derraik, J. G., Anderson, W. A., Connelly, E. A. & Anderson, Y. C. Rapid evidence
470 summary on SARS-CoV-2 survivorship and disinfection, and a reusable PPE protocol
471 using a double-hit process. *MedRxiv* (2020).

472 36. Bouvier, N. M. & Palese, P. The biology of influenza viruses. *Vaccine* **26**, D49-D53
473 (2008).

474 37. Bar-On, Y. M., Flamholz, A., Phillips, R. & Milo, R. Science Forum: SARS-CoV-2
475 (COVID-19) by the numbers. *Elife* **9**, e57309 (2020).

476 38. Wang, X., Zoueva, O., Zhao, J., Ye, Z. & Hewlett, I. Stability and infectivity of novel
477 pandemic influenza A (H1N1) virus in blood-derived matrices under different storage
478 conditions. *BMC infectious diseases* **11**, 1-6 (2011).

39. Tomb, R. M. *et al*. Inactivation of Streptomyces phage ϕC31 by 405 nm light: Requirement for exogenous photosensitizers? *Bacteriophage* **4**, e32129 (2014).

40. Richardson, T. B. & Porter, C. D. Inactivation of murine leukaemia virus by exposure to visible light. *Virology* **341**, 321-329 (2005).

41. Girard, P. et al. *UVA-induced damage to DNA and proteins: direct versus indirect photochemical processes* (Journal of Physics: Conference Series Ser. 261, IOP Publishing, 2011).

42. IEC 62471:. Photobiological safety of lamps and lamp systems. (2006).

43. Dougall, L. R., Anderson, J. G., Timoshkin, I. V., MacGregor, S. J. & Maclean, M. *Efficacy of antimicrobial 405 nm blue-light for inactivation of airborne bacteria* (Light-Based Diagnosis and Treatment of Infectious Diseases Ser. 10479, International Society for Optics and Photonics, 2018).

44. Nardell, E. A. *et al*. Safety of upper-room ultraviolet germicidal air disinfection for room occupants: results from the Tuberculosis Ultraviolet Shelter Study. *Public Health Rep.* **123**, 52-60 (2008).